Structural Analysis of Small-Molecule Binding to the BAZ2A and BAZ2B Bromodomains

Andrea Dalle Vedove,[a] Dimitrios Spiliotopoulos,[b] Vito G. D'Agostino,[a] Jean-Rémy Marchand,[b] Andrea Unzue,[c] Cristina Nevado,[c] Graziano Lolli,*[a] and Amedeo Caflisch*[b]

The bromodomain-containing protein BAZ2A is a validated target in prostate cancer research, whereas the function of its paralogue BAZ2B is still undefined. The bromodomains of BAZ2A and BAZ2B have a similar binding site for their natural ligand, the acetylated lysine side chain. Here, we present an analysis of the binding modes of eight compounds belonging to three distinct chemical classes. For all compounds, the moiety mimicking the natural ligand engages in essentially identical interactions in the BAZ2A and BAZ2B bromodomains. In contrast, the rest of the molecule is partially solvent-exposed and adopts different orientations with different interactions in the two bromodomains. Some of these differences could be exploited for designing inhibitors with selectivity within the BAZ2 bromodomain subfamily.

Introduction

Bromodomains are epigenetic reader modules that recognize acetylated lysine (Kac) residues in histones and other proteins; they are associated with additional domains involved in chromatin remodeling and transcriptional regulation (histone acetylases, methyltransferases, transcription factors, and helicases).[1]

Bromodomain adjacent to zinc finger domain protein 2A (BAZ2A) is over-expressed in prostate cancer (PCa), inducing aberrant gene silencing.[2] BAZ2A expression correlates both with PCa aggressiveness and recurrence and with the evolution of a metastatic phenotype. Invasion and migration of metastatic PCa cells are drastically impaired upon BAZ2A knockdown. The chromatin template activities of BAZ2A mediate its oncogenic effects, making its bromodomain a promising target to interfere with PCa progression and recurrence. BAZ2A induces aberrant gene silencing in PCa also in cooperation with enhancer of zest homologue 2 (EZH2), the altered expression of which is linked to malignancy and poor prognosis.[3] Three EZH2 inhibitors are currently being tested in clinical trials.[4]

The bromodomain of BAZ2B shares a similar Kac-binding site (76% sequence identity and 93% similarity) with its paralogue BAZ2A. The physiological function of BAZ2B is still unknown, whereas single nucleotide polymorphisms in the BAZ2B gene locus have been associated with sudden cardiac death.[5]

The first fragment binders for BAZ2B were identified by Ciulli and co-workers in 2013.[6] In contrast to the members of the bromo and extraterminal (BET) domain subfamily of human bromodomains, for which many potent and selective inhibitors have been developed (11 are currently being tested in clinical trials),[4] the BAZ2 bromodomains have a shallow Kac-binding pocket with only two potent inhibitors developed thus far, which are unable to discriminate between the two paralogues.[7,8]

Here we report eight crystallographic structures of small molecules from three different chemical classes in complex with the BAZ2A bromodomain; structures for seven of those molecules in complex with the bromodomain of BAZ2B were also determined. Comparison of those structures has allowed the identification of common and divergent features in the binding modes of fragments/small molecules to the two BAZ2 bromodomains, providing additional hints for the development of specific BAZ2A or BAZ2B bromodomain inhibitors. Additionally, one of the BAZ2A structures derives from a novel crystallographic packing and space group and was determined at a resolution of 1.1 Å, constituting the highest resolution structure for this bromodomain determined to date.

Results and Discussion

The eight small molecules selected for structural studies in complex with BAZ2A and BAZ2B belong to three different chemical classes (Table 1). The 1-methylpyridinones **1**–**5** were
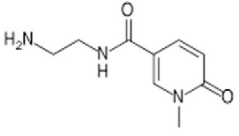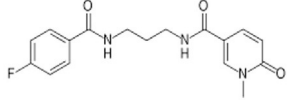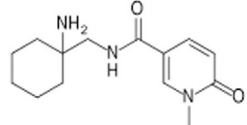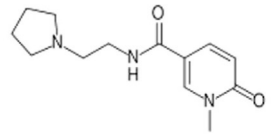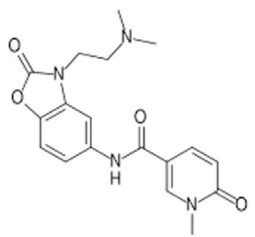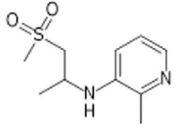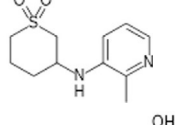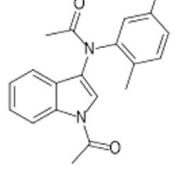
[a] Dr. A. Dalle Vedove, Dr. V. G. D'Agostino, Dr. G. Lolli
Centre for Integrative Biology, University of Trento, via Sommarive 9, 38123, Povo-Trento (Italy)
E-mail: graziano.lolli@unitn.it

[b] Dr. D. Spiliotopoulos, Dr. J.-R. Marchand, Prof. A. Caflisch
Department of Biochemistry, University of Zürich, Winterthurerstrasse 190, 8057, Zürich (Switzerland)
E-mail: caflisch@bioc.uzh.ch

[c] Dr. A. Unzue, Prof. C. Nevado
Department of Chemistry, University of Zürich, Winterthurerstrasse 190, 8057, Zürich (Switzerland)

Supporting information and the ORCID identification number(s) for the author(s) of this article can be found under: https://doi.org/10.1002/cmdc.201800234.

Table 1. Binding activity for compounds **1**–**8**.

Compound	BAZ2A				BAZ2B			
	% Ctrl[a]	IC$_{50}$ [µM][b]	K_d [µM][c]	PDB ID	% Ctrl[a]	IC$_{50}$ [µM][b]	K_d [µM][c]	PDB ID
1	73	>820	>400	6FG6	59	>1000	–	6FH6
2	84	>1000	110	6FGF	90	>1000	–	6FH7
3	>90	–	–	6FGV	68	–	–	6FGT
4	57	–	–	6FGW	69	–	–	6FGU
5	25	88	17	6FGG	19	89	–	–
6	21	–	–	6FGH	7	>500[d]	–	5L96
7	21	–	–	6FGI	4	279[d]	–	5L8T
8	42	24	–	6FGL	29[a] 54[e]	8	23[f]	5E73

Dashes indicate data were not acquired. [a] Residual binding of the H3K(Ac)14 peptide at 1 mM compound concentration measured by AlphaScreen; lower percentage values indicate tighter binding of the compound. [b] Determined by AlphaScreen. [c] Determined by BROMOscan. [d] Reported in Ref. [10], determined by Alphascreen. [e] Residual binding at 0.05 mM measured by AlphaScreen in Ref. [11]. [f] Reported in Ref. [11], determined by BROMOscan. Compounds **6** and **7** were tested as racemic mixtures.

prioritized following in silico screening and competition binding assays, starting from a parent fragment identified in a previous screening campaign.[9] The 3-amino-2-methylpyridine derivatives **6**–**7** and the acetylindole compound **8** had been identified previously as BAZ2B ligands and they represent interesting molecules for further optimization of their potency and selectivity.[10,11] We first present the results of a substructure search (fragment **1** from Ref. [9]) followed by a comparison of

the binding sites of BAZ2A and BAZ2B, and then we analyze the differences in binding modes and interaction motifs.

Substructure search

With the aim of increasing specificity for BAZ2A versus BAZ2B, we performed a substructure search using the *N*-methyl-2-pyridone-5-carboxamide head (from fragment **1** in Ref. [9]) as a

query on the ZINC15 database. This search yielded 444 compounds that include a positively charged, H-bond donor or halogen-bond donor tail, that can reach the BAZ2A Glu1820 side chain (the corresponding residue in BAZ2B is Leu1891). These compounds were docked to the BAZ2A structure from the complex with fragment **1** of Ref. [9] (PDB ID: 5MGJ) using the program SEED.[12,13] In all BAZ2A structures available at the time, Glu1820 adopted the mm rotameric form ($\chi = -65°$). On the other hand, we noticed that this residue is not involved in any intramolecular interactions and, for docking, we changed it to the pt rotamer ($\chi = 63°$), which points toward the interior of the cavity, emulating an induced fit. Charged compounds were ranked according to the electrostatic energy, whereas uncharged compounds according to consensus scoring as in our previous work (see the Experimental Section). A total of 22 compounds (14 with a positively charged amino group and eight noncharged) were selected and tested for BAZ2A binding at a single dose in the AlphaScreen assay (Table S1 in the Supporting Information). Dose–response curves of the most active compounds were then obtained using the AlphaScreen assay and/or the BROMOScan assay (Table 1 and Figures S1 and S2). Compound **5** was the most active against the BAZ2A bromodomain in both assays with an IC_{50} value of 88 μM and a K_d of 17 μM. It has been reported by several groups that the K_d values measured by the BROMOscan assay are up to an order of magnitude more favorable than the IC_{50} values obtained by AlphaScreen.[14–17] Overall, the substructure search resulted in five new crystal structures but only a modest improvement of affinity with respect to the original hit (from a K_d of 51 μM for fragment **1** of Ref. [9] to a K_d of 17 μM for ligand **5** in this work).

The structure of the bulky compound **5** in complex with BAZ2B could not be determined; packing constraints impeded binding of the compound by soaking, whereas co-crystallization attempts yielded no crystals. In contrast, binding of the compound in BAZ2A induced a new crystallographic packing through the stacking of two symmetry-related 2-benzoxazolinone moieties bound to two neighboring protein chains (Figure S3). The X-ray structure was determined at a 1.1 Å resolution, which represents the highest resolution structure for the BAZ2A bromodomain obtained to date. The new orthorhombic crystallographic packing had no influence on the pose of compound **5**, as a similar binding mode was observed in the significantly lower resolution structure (3.0 Å, not shown), which was obtained by soaking the usual trigonal crystal form in the compound solution. The only difference resides in the highly degraded electron density for the terminal *N,N*-dimethylethylamino group in the lower resolution structure. The slightly higher affinity of compound **5** with respect to the other 1-methylpyridinone derivatives **1**–**4** can be explained by the T-shaped π–π stacking interaction between the 2-benzoxazolinone ring and Trp1816 (Figure 1). Moreover, the *N,N*-dimethylamino substituent of compound **5** is involved in additional van der Waals interactions with the aforementioned tryptophan residue, whereas the non-optimal geometry makes questionable whether a cation–π interaction between the same groups also favorably contributes to the binding energy. The
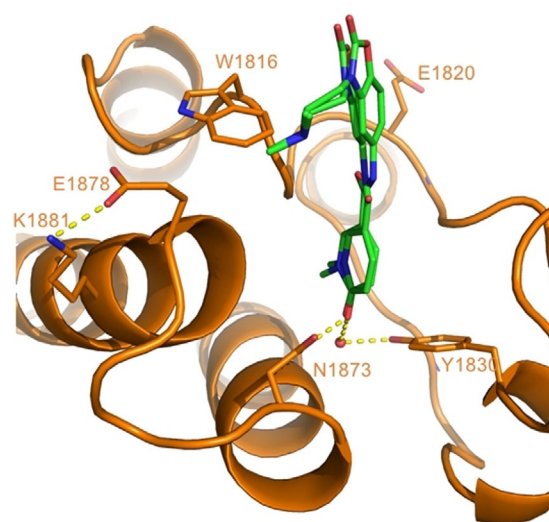

Figure 1. Binding mode of compound **5**. The amide linker of compound **5** (green) can assume two conformations in the BAZ2A pocket.

terminal dimethylamino group is also in close proximity to Glu1878, which would need to switch to a different conformer in order to establish an ionic interaction; such a rearrangement was not observed, and Glu1878 remains involved in the intramolecular electrostatic interaction with Lys1881, as observed in the other BAZ2A structures.

Comparison of BAZ2A and BAZ2B binding sites

The holo structures of BAZ2A and BAZ2B presented here show common features irrespective of the bound inhibitor. The Kac-binding sites have similar parallelepiped-like shape largely defined by the ZA loop (residues 1813–1838 in BAZ2A and 1884–1909 in BAZ2B) and BC loop (residues 1873–1877 in BAZ2A and 1944–1948 in BAZ2B). In complexes with different ligands, the BAZ2A bromodomain shows no significant structural deviations in the loops. Upon superposition over all Cα atoms, the maximal pairwise RMSD was 0.56 Å for Cα atoms in the BC loop and 0.70 Å for Cα atoms in the ZA loop (Figure 2a). In BAZ2B structures, a larger flexibility is observed for the ZA loop, whereas the BC loop, similarly to BAZ2A, shows limited positional variability (maximal pairwise RMSD of 0.44 Å for Cα atoms in the BC loop and 1.34 Å for Cα atoms in the ZA loop, Figure 2b). The plasticity of the ZA loop emerges also from the structural overlap of the two bromodomains with a deviation as large as 1.8 Å between the Cα atoms of Leu1826 in BAZ2A and the corresponding BAZ2B Leu1897 residue (in complex with compound **8**, PDB IDs: 6FGL and 5E73), whereas the largest deviation in the BC loop is smaller than 1.0 Å (Figure 2c). The higher disorder of the ZA loop in BAZ2B might originate, at least in part, from the presence of Pro1824 in BAZ2A whose corresponding residue is Leu1895 in BAZ2B. On the other hand, the crystal packing could differently influence loops flexibility in the two bromodomains, an effect that is difficult to weight accurately.
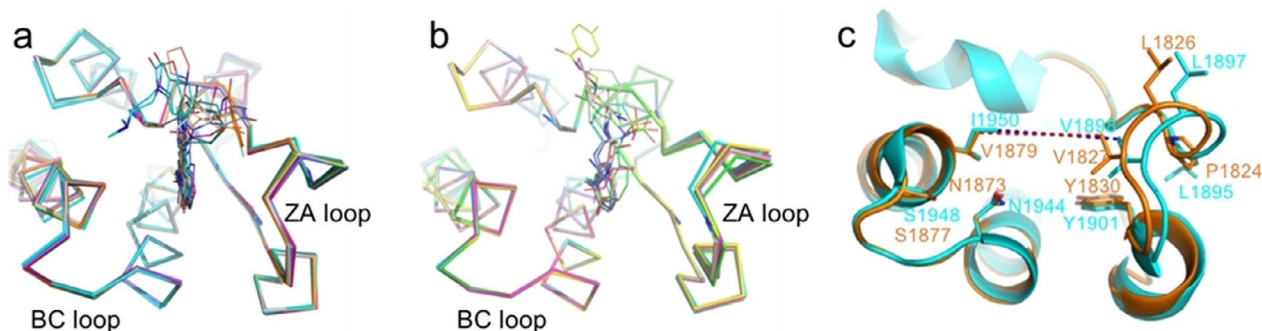
Figure 2. Flexibility and structural variations in BAZ2A and BAZ2B bromodomains. a) Superposition of BAZ2A structures in complex with compounds **1–8** (Table 1) shows limited variability in the BC and ZA loops. b) Superposition of BAZ2B structures in complex with compounds **1–4** and **6–8** shows the higher flexibility of the ZA loop. c) Binding site aperture and distances between main interaction motifs in BAZ2A and BAZ2B bromodomains. BAZ2A (PDB ID: 6FGL, orange) and BAZ2B (PDB ID: 5E73, cyan) structures deviate significantly from each other at the tip of the ZA loop (Leu1826 in BAZ2A and Leu1897 in BAZ2B); superposition is shown for structures in complex with compound **8**. The substitution of Pro1824 in BAZ2A to Leu1895 in BAZ2B might determine the observed divergence as well as the larger flexibility of the loop in BAZ2B. Another relevant difference between the Kac pockets of the two bromodomains resides in the gatekeeper residues: Val1879 in BAZ2A and Ile1950 in BAZ2B. The aperture of the binding site is similar in the two bromodomains, as shown by the dashed lines connecting the tip of the side chains of the gatekeeper residue and the opposite valine residue (BAZ2A: Val1879–Val1827, red dashed line; BAZ2B: Ile1950–Val1898, blue dashed line).

BAZ2A seems to have a reduced binding site aperture with respect to BAZ2B if one considers the distances between corresponding pairs of backbone atoms in the two loops. However, a more detailed analysis reveals that the effective space available to the ligand is essentially identical in the two bromodomains, because the distance between the two side chains that protrude from the two loops to the center of the binding site is, in both cases, approximately 8.3 Å, as measured between the tip of the gatekeeper side chain and the ZA loop Val1827 or Val1898 (in BAZ2A or BAZ2B, respectively, Figure 2c).

Comparison of binding modes

In the deepest part of the pocket, that is, the part that recognizes the acetyl moiety of Kac, the acetyl oxygen atom forms hydrogen bonds with the side chains of the evolutionary conserved Asn1873 and Tyr1830 in BAZ2A (Asn1944 and Tyr1901 in BAZ2B); the latter interaction involves a structurally conserved water molecule (W1) acting as a bridge. Both hydrogen bonds are present in all crystal structures of BAZ2A/B reported in this work, as well as in those previously disclosed with the exception of the complex between BAZ2B and 6-hydroxyindole in which the NH of the ligand replaces the water W1 (PDB ID: 5E9I).[18] The scatter plot in Figure 3a shows that the
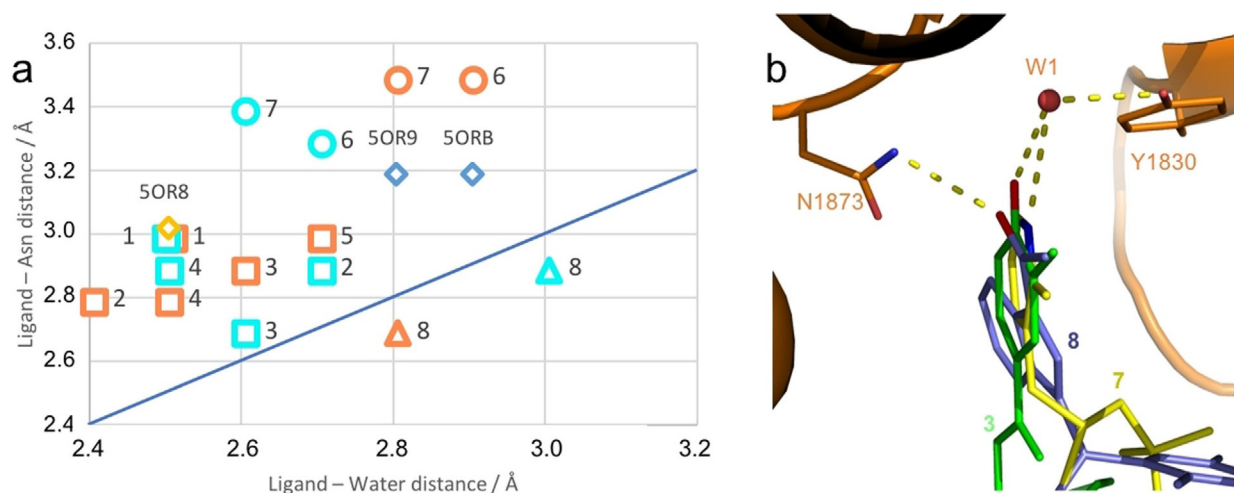

Figure 3. Binding modes in the acetyl-recognition region of BAZ2A and BAZ2B Kac pockets. a) Scatter plot of the hydrogen bond lengths between compounds **1–8** (Table 1) and the conserved asparagine residue (Asn1873 in BAZ2A and Asn1944 in BAZ2B) and a water molecule at the bottom of the Kac pocket of the two bromodomains. Numbers denote the ligand, symbols the chemical class (squares, 1-methylpyridinones **1–5**; circles, 3-amino-2-methylpyridine derivatives **6–7**; triangle, acetylindole **8**), and color the bromodomain (orange, BAZ2A; cyan, BAZ2B). Distances for the 1,3-dimethyl-benzimidazolone (in complex with BAZ2A, PDB ID: 5OR8; light-orange diamond) and the two 1-methyl-cyclopentapyrazole derivatives (in complex with BAZ2B, PDB IDs: 5ORB and 5OR9; blue diamonds), which were recently described,[29] are also included. Note that compounds **6**, **7**, and the ligands in the PDB structures 5ORB and 5OR9 have a nitrogen atom in an aromatic ring as hydrogen bond acceptor, whereas all other compounds have a carbonyl oxygen atom. b) Hydrogen bond pattern at the bottom of the BAZ2A Kac pocket, represented for the different chemical classes. 1-Methylpyridinone (**3**, green) and 3-amino-2-methylpyridine (**7**, yellow) derivatives form a hydrogen bond with the conserved water molecule W1; the acetylindole derivative **8** (purple) is closer to Asn1873 than to W1.

distance to the bridging water is shorter than the distance to the side chain of the conserved asparagine for all compounds (except for the acetylindole derivative **8**) in agreement with previous reports.[14, 19, 20] Interestingly, the hydrogen bond lengths can be clustered on the basis of the chemical class of the compounds independently of the bound bromodomain. The distance to the structurally conserved water reflects the degree of burial of the compounds (Figure 3 b). The 1-methyl-pyridinone compounds **1**–**5** bind deeper in the Kac pocket than compounds from the other chemical classes. The hydrogen bond length to the side-chain NH_2 group of the conserved Asn is relatively large (3.2 to 3.5 Å) for the ligands with an aromatic nitrogen atom (pyridine) acting as hydrogen-bond acceptor (**6**, **7**, and the ligands in structures 5OR9 and 5ORB), whereas it is significantly shorter (2.7 to 3.0 Å) for all other compounds that have a carbonyl oxygen atom as an acceptor, as well as for the hydroxy oxygen atom of 1,2-ethanediol in BAZ2A (PDB ID: 4LZ2).

In the middle part of the cavity, the difference in the gate-keeper residue, Val1879 in BAZ2A and Ile1950 in BAZ2B, induces tilting of the aromatic ring constituting the head group of the various molecules reported here. The influence of the gate-keeper residue on the orientation of small-molecule ligands in the Kac binding site has been reported previously.[11] The observed tilting is only approximately 10 degrees in compounds **6**–**7** that contain the small 2-methylpyridine head group (Figure 4 a), in which the anchoring nitrogen atom is part of the aromatic ring (a pyridine), and more pronounced (between 15 and 25 degrees, depending on the inhibitor, Figure 4 b) in the case of the more protruding and larger 1-methylpyridinone and acetylindole head groups in compounds **1**–**4** and **8**, respectively.

The largest differences in BAZ2A/B binding are observed for the tail moiety, as evident for compounds **1**, **2**, and **8** (Figure 5). In BAZ2B, the ethylenediamine tail of compound **1** closely follows the path of the Kac residue in histone peptides
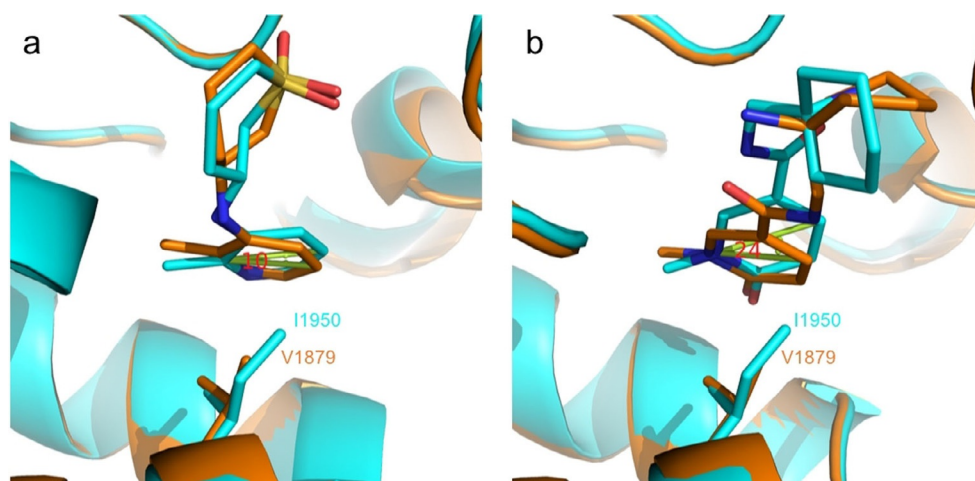

Figure 4. The tilting of head groups induced by the gatekeeper residues varies with the chemical scaffold of the ligand. a) The head group in compound **7** is tilted by only 10° in BAZ2B (cyan) with respect to BAZ2A (orange). The angle of the aromatic planes is shown by two segments (green with angle value in red). b) Tilting is more pronounced in compound **3** (24°; color code as above).
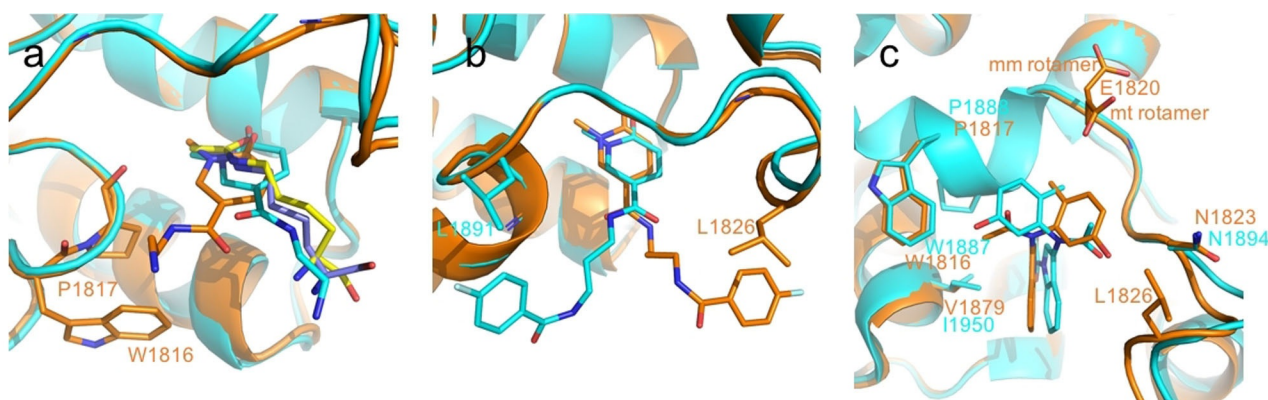

Figure 5. Similar binding modes of head groups to BAZ2A (orange) and BAZ2B (cyan) and differences in the tail groups. a) The binding mode of compound **1** to BAZ2B is similar to that of Kac to BAZ2A (PDB ID: 4QBM, yellow) and BAZ2B (PDB ID: 4QC1, purple). The tail of compound **1** is oriented differently in BAZ2A and BAZ2B. b) The tail of compound **2** is oriented in opposite directions in BAZ2A and BAZ2B. c) The positions of the two substituents in compound **8** are inverted in BAZ2A and BAZ2B. The side chain of Glu1820 in BAZ2A is present in double conformation assuming the mm and mt rotamers.

bound to BAZ2A and BAZ2B (PDB IDs: 4QBM, 4QC1, and 4QC3);[21] in BAZ2A, the same tail is rotated by approximately 60° and is close to Trp1816 and Pro1817 of the WPF shelf (Figure 5a). The divergence can be exacerbated by differences in sequence and structure between BAZ2A and BAZ2B in the more external part of the Kac binding pocket. Compound **2** binds to BAZ2A with its fluorophenyl tail in hydrophobic contact with Leu1826 at the tip of the ZA loop (Figure 5b). In BAZ2B, the tail is rotated by about 180° and the fluorophenyl moiety is in contact with Leu1891, which corresponds to Glu1820 in BAZ2A. The crystallographic packing does not influence the orientation of compound **2** in either bromodomain structure.

Compound **8** shows substantial differences in its binding mode to the two BAZ2 bromodomains (Figure 5c). The 3-amino-1-acetylindole head group is tilted due to the difference in the gatekeeper residue. The head group bears two additional substituents on the nitrogen atom in position 3, which are different in size: a small acetyl group and a bulkier 2-methyl-5-hydroxybenzene ring. The two substituents are oriented in opposite directions in the two bromodomains. In BAZ2A, the smaller gatekeeper Val1879 holds the acetylindole ring close to the WPF shelf so that the acetyl group is in van der Waals contact with Trp1816 and Pro1817, whereas the 2-methyl-5-hydroxybenzene ring is oriented toward Asn1823 and Leu1826 on the tip of the ZA loop. In BAZ2B, the gatekeeper Ile1950 pushes the acetylindole ring away from the WPF shelf; the 2-methyl-5-hydroxybenzene ring is now in contact with Trp1887 and Pro1888, and the acetyl group occupies the reduced space (in comparison with BAZ2A) toward the tip of the ZA loop and also forms a hydrogen bond with the main-chain nitrogen atom of Asn1894.

Selectivity filters in BAZ2A

Two variations in sequence between BAZ2A and BAZ2B— Val1879 to Ile1950 (Figure 4, the gatekeeper residue) and Glu1820 to Leu1891—are putative selectivity determinants that were not fully investigated for the compounds reported here. Despite having interesting differences in their binding modes to BAZ2A and BAZ2B, similar affinities for both bromodomains were measured for all tested compound (Table 1 and Table S1).

For ligands **1**–**4**, the tails are involved in a limited number of contacts with the protein matrices; moreover, the electron density rapidly decreases toward the more external part of the inhibitors, indicating high flexibility and possible multiple conformations for these tails. The positively charged tails of compounds **1**, **3**, and **4** bound to BAZ2A are correctly oriented toward Glu1820 (Leu1891 in BAZ2B), but are too flexible and short to be involved in electrostatic interactions (Figure 6). Nevertheless, they represent interesting vectors to investigate this difference in sequence. The tail of compound **5** contacts residues that are conserved between the two bromodomains and the mode of binding to BAZ2B would likely be similar to that observed with BAZ2A (Figure 1). In BAZ2A, the positively charged tail of ligand **5** is oriented toward Glu1878 and thus
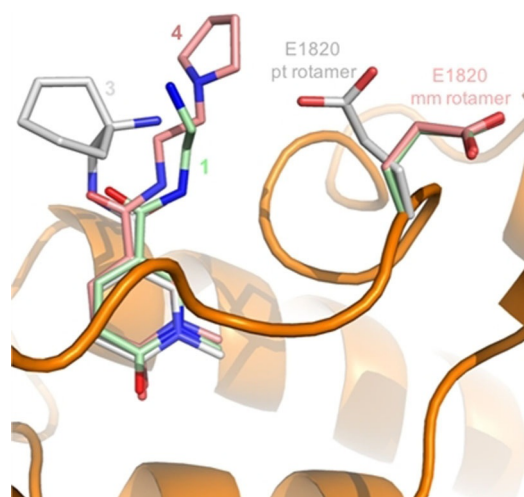

Figure 6. Orientations of ligand tail groups in BAZ2A and the Glu1820 side chain. Compounds **1**, **3**, and **4** (light green, gray, and pink, respectively) bind to BAZ2A with different orientations of the tail groups. In the complex with compound **3**, Glu1820 assumes the pt rotameric state (gray).

points in the opposite direction with respect to the side chain of Glu1820. Substitutions in different positions of an aromatic ring that acts as spacer (like the 2-benzoxazolinone of compound **5**) could prove useful in correctly reorienting a terminal positively charged group toward Glu1820 while maintaining the π–π stacking interaction with Trp1816.

Compounds **6** and **7** show similar binding modes in the two bromodomains (Figure 4a). Despite containing a stereogenic center, a single enantiomer is present or at least largely predominant in the X-ray structures in complex with BAZ2B.[10] The lower resolution of the BAZ2A crystallographic structures makes questionable whether a similar specificity is possible also for this bromodomain, in which the smaller gatekeeper residue might result in a less stringent enantiomeric selectivity, a possibility worth further investigation.

In compound **8**, the bipartite tail assumes inverted orientations in the two bromodomains as a consequence of the differential tilt imposed on the inhibitor by the gatekeeper residues. Asymmetry and bulkiness of the two substituents of the tail could then be exploited to gain selectivity for BAZ2A, as well as appropriate functional groups to complement the different charge distribution of the bromodomains; in BAZ2A, the 2-methyl-5-hydroxybenzene substituent is close to Glu1820 (Figure 5c).

Finally, the side chain of Glu1820 in BAZ2A can assume conformations other than the reported mm rotamer. In the complexes with compounds **3** and **8**, Glu1820 is present as a pt rotamer (the one selected for the protein model used in the docking procedure) and mt rotamer, respectively (Figure 5c and 6). Both pt and mt rotamers point toward the interior of the binding cavity, providing evidence that the interaction with Glu1820 can be exploited to determine the specificity for small molecules binding to BAZ2A versus BAZ2B.

Conclusions

We present eight new structures of the BAZ2A bromodomain in complex with small molecules that originate from the expansion of fragment hits identified by docking. Whereas the BAZ2A/B ligands **6**–**8** were reported previously,[10, 11] compounds **1**–**5** are disclosed here for the first time. They are derivatives of the N-methyl-2-pyridone-5-carboxamide head group (i.e., fragment **1** of Ref. [9]), that were identified by substructure searches and docking with evaluation of binding energy using a force field energy with electrostatic desolvation effects. Compound **5** showed a slightly higher binding affinity to BAZ2A with respect to compounds **1**–**4** and to the parent fragment (**1** of Ref. [9]). The complex with compound **5** was determined in a new space group and crystallographic packing, and constitutes the highest resolution structure for the BAZ2A bromodomain to date. The eight holo structures of BAZ2A supplement the seven structures already deposited in the PDB (the apo structure, the complex with the acetylated H4 peptide, and five complexes with fragments/small molecules), and together they constitute a large dataset for a detailed description of small molecules binding to the Kac binding site of BAZ2A.

We focused the analysis on the comparison with the similar pocket of the cognate BAZ2B bromodomain, for which many holo structures are available in the PDB. Structures of seven small molecules are available in complex with both bromodomains (four of them in complex with BAZ2B also reported here for the first time). Four main observations emerge from the comparative analysis. First, the slightly lower flexibility observed for the ZA loop in BAZ2A is likely due to the presence of Pro1824, of which the corresponding BAZ2B residue is Leu1895. Second, in the deepest part of the pocket, residues are conserved between the two bromodomains, and the anchoring of the head group is largely determined by its chemical identity and shape. Third, the difference in the gatekeeper residue induces a tilting of the head group (Kac mimic), which can influence the orientation of the substituents (e.g., compound **8**, Figure 5c). Fourth, the BAZ2A Glu1820 side chain (the corresponding BAZ2B residue of which is Leu1891) can assume rotameric configurations that direct its negative charge toward the Kac pocket, which suggests that this residue can be exploited as a specificity determinant for the binding of small molecules to BAZ2A versus BAZ2B.

Experimental Section

Substructure search, docking, and ranking: A library of 444 molecules was obtained by substructure search using the N-methyl-2-pyridone-5-carboxamide (the head group of compound **1** in Ref. [9]) as a query on the ZINC15 database. Compounds that did not include a positively charged, hydrogen-bonding, or halogen-bonding donor tail, theoretically capable of reaching the BAZ2A Glu1820 side chain, or those that presented unwanted substitutions on the head group (i.e., in position 6) were discarded. The molecular weights of these molecules range from 166.1 to 412.2 g mol^{-1} with a median of 252.2 g mol^{-1}. The number of rotatable bonds ranges from 1 to 12 with a median of 4. The number of hydrogen-bond donors and acceptors ranges from 0 to 3 with a median of 1 and from 1 to 6 with a median of 4, respectively.

For each of the 444 N-methyl-2-pyridone-5-carboxamide derivatives (96 have a positively charged amino group and 348 are non-charged), 100 conformers were generated, relying on the RDKit[22] and parametrized using CGenFF.[23, 24] The program SEED[12, 13] was used for docking a total of 44 400 conformers to the BAZ2A structure (PDB structure 5MGJ with Glu1820 in the pt rotameric configuration). The poses of the charged compounds were ranked according to the electrostatic interaction energy with approximation of solvent screening effects by the generalized Born model with numerical evaluation of the Born radii.[25] The uncharged molecules were ranked according to consensus scoring using the median rank of three energy terms as in our previous work[9] with the difference that the van der Waals efficiency was counted twice, that is, weighted twice with respect to each of the two remaining terms—electrostatic difference and SEED total energy. Double-weighting the van der Waals efficiency favors small molecules with a small number of non-hydrogen atoms.

Compound purity: Compounds **1**–**7** were purchased from Enamine (Riga, Latvia). Compound **8** was synthesized as previously described.[11] The molecules were determined to be ≥95% pure by HPLC–MS and NMR spectroscopy.

Protein expression and purification: BAZ2AA-c002 was a gift from Nicola Burgess-Brown (Addgene plasmid #53623). For crystallization purposes, BAZ2A (residues 1796–1899) and BAZ2B (residues 1858–1972) bromodomains were produced as previously described.[9] In brief, proteins were purified by immobilized metal-affinity chromatography (IMAC), followed by buffer exchange, tag removal by TEV protease, a second round of IMAC and size-exclusion chromatography. For the AlphaScreen assay, bromodomains were left with the His$_6$ tag and then subjected to size-exclusion chromatography using a Superdex 75 column, immediately after the first purification step by IMAC.

AlphaScreen assay: Recombinant His-tagged BAZ2A and BAZ2B bromodomains were tested in house by Alpha technology in the presence of a biotinylated histone H3 acetylated lysine 14 peptide [H3K(Ac)14, H-YQTARKSTGGK(Ac)APRKQLATKAK(Biotin)-OH][26] using the AlphaScreen histidine detection kit (PerkinElmer). The assays were performed in 384 optiplates (PerkinElmer) as previously described[27] using equimolar amount of ligands at the hooking point (750 nM) evaluated after incubation for 1 h at room temperature in buffer A (50 mM HEPES, pH 7.4, 100 mM NaCl, 0.1% BSA, 0.05% CHAPS). Compounds, dissolved in DMSO, were tested in duplicate and dose–response and IC$_{50}$ values were obtained by nonlinear regression of log(dose)–response fit using GraphPad Prism software v5.1. DMSO was kept below 2% as final concentration and data were normalized against corresponding DMSO controls.

BROMOscan assay: Assays were performed at DiscoverX (Fremont, CA, USA) with the BROMOscan profiling service. BROMOscan is a competition-based technology using a ligand immobilized to a solid support and DNA-tagged bromodomains. Bromodomains were incubated with the ligand in the presence and absence of the putative inhibitors and eluted for quantification by qPCR. Small molecules inhibiting the binding of the bromodomain to the immobilized ligand will reduce the amount of bromodomain captured and thus the qPCR signal.[28] The ligand used for the assay is proprietary and undisclosed. Dissociation constants (K_d) were calculated by fitting a 12-point dilution curve with starting concentration in the range 0.2–0.4 mM (depending on solubility of the com-

pound) and a dilution factor of 3.0. All dose–responses were measured in duplicate.

Crystallization, data collection and structure solution: Co-crystallization of BAZ2A with the compounds of interest and crystallization and soaking for the BAZ2B bromodomain were performed as previously described.[29] Compounds were dissolved in crystallization or soaking solutions devoid of DMSO, which binds in the Kac pocket of bromodomains.[18,30]

Diffraction data were collected at the Elettra Synchrotron Light Source (Trieste, Italy), XRD1 beamline (PDB IDs: 6FG6, 6FGF, 6FGG, 6FGH, 6FGI, 6FGL, 6FGT, 6FGU, 6FGV and 6FGW) and at the Swiss Light Source, Paul Scherrer Institute (Villigen, Switzerland), beamline PXI (PDB IDs: 6FH6 and 6FH7). Data were processed with XDS[31] and Aimless;[32] the high-resolution cutoff was selected according to Karplus and Diederichs.[33] BAZ2B crystals soaked with compounds **1** and **2** (PDB IDs: 6FH6 and 6FH7, respectively) were strongly anisotropic: ellipsoidal diffraction data were treated by making use of the STARANISO server (http://staraniso.globalphasing.org/cgi-bin/staraniso.cgi). Structures were solved by molecular replacement with Phaser[34] using the PDB structure 4IR5 as a search model for BAZ2B and 5MGJ for BAZ2A. Initial models were refined by alternating cycles of automatic refinement with Phenix[35] and manual model building with COOT.[36]

Data collection and refinement statistics are reported in Tables S2 and S3. Electron densities are shown in Figure S4 for compounds **1**–**8** in all structures reported here.

Accession codes: BAZ2A structures were deposited in the Protein Data Bank with accession numbers 6FG6 (co-crystallized with compound **1**), 6FGF (compound **2**), 6FGV (compound **3**), 6FGW (compound **4**), 6FGG (compound **5**), 6FGH (compound **6**), 6FGI (compound **7**), and 6FGL (compound **8**). BAZ2B structures were deposited in the PDB with accession numbers 6FH6 (co-crystallized with compound **1**), 6FH7 (compound **2**), 6FGT (compound **3**), and 6FGU (compound **4**). Atomic coordinates and experimental data will be released upon publication of this article.

Acknowledgements

Conflict of interest

The authors declare no conflict of interest.

[1] P. Filippakopoulos, S. Knapp, *Nat. Rev. Drug Discovery* **2014**, *13*, 337–356.

[2] L. Gu, S. C. Frommel, C. C. Oakes, R. Simon, K. Grupp, C. Y. Gerig, D. Bär, M. D. Robinson, C. Baer, M. Weiss, Z. Gu, M. Schapira, R. Kuner, H. Sültmann, M. Provenzano, ICGC Project on Early Onset Prostate Cancer, M. L. Yaspo, B. Brors, J. Korbel, T. Schlomm, G. Sauter, R. Eils, C. Plass, R. Santoro, *Nat. Genet.* **2015**, *47*, 22–30.

[3] S. Varambally, S. M. Dhanasekaran, M. Zhou, T. R. Barrette, Kumar-C. Sinha, M. G. Sanda, D. Ghosh, K. J. Pienta, R. G. Sewalt, A. P. Otte, M. A. Rubin, A. M. Chinnaiyan, *Nature* **2002**, *419*, 624–629.

[4] https://clinicaltrials.gov.

[5] D. E. Arking, M. J. Junttila, P. Goyette, A. Huertas-Vazquez, M. Eijgelsheim, M. T. Blom, C. Newton-Cheh, K. Reinier, C. Teodorescu, A. Uy-Evanado, N. Carter-Monroe, K. S. Kaikkonen, M. L. Kortelainen, G. Boucher, C. Lagacé, A. Moes, X. Zhao, F. Kolodgie, F. Rivadeneira, A. Hofman, J. C. Witteman, A. G. Uitterlinden, R. F. Marsman, R. Pazoki, A. Bardai, R. W. Koster, A. Dehghan, S. J. Hwang, P. Bhatnagar, W. Post, G. Hilton, R. J. Prineas, M. Li, A. Köttgen, G. Ehret, E. Boerwinkle, J. Coresh, W. H. Kao, B. M. Psaty, G. F. Tomaselli, N. Sotoodehnia, D. S. Siscovick, G. L. Burke, E. Marbán, P. M. Spooner, L. A. Cupples, J. Jui, K. Gunson, Y. A. Kesäniemi, A. A. Wilde, J. C. Tardif, C. J. O'Donnell, C. R. Bezzina, R. Virmani, B. H. Stricker, H. L. Tan, C. M. Albert, A. Chakravarti, J. D. Rioux, H. V. Huikuri, S. S. Chugh, *PLoS Genet.* **2011**, *7*, e1002158.

[6] F. M. Ferguson, O. Fedorov, A. Chaikuad, M. Philpott, J. R. Muniz, I. Felletar, F. von Delft, T. Heightman, S. Knapp, C. Abell, A. Ciulli, *J. Med. Chem.* **2013**, *56*, 10183–10187.

[7] P. Chen, A. Chaikuad, P. Bamborough, M. Bantscheff, C. Bountra, C. W. Chung, O. Fedorov, P. Grandi, D. Jung, R. Lesniak, M. Lindon, S. Müller, M. Philpott, R. Prinjha, C. Rogers, C. Selenski, C. Tallant, T. Werner, T. M. Willson, S. Knapp, D. H. Drewry, *J. Med. Chem.* **2016**, *59*, 1410–1424.

[8] L. Drouin, S. McGrath, L. R. Vidler, A. Chaikuad, O. Monteiro, C. Tallant, M. Philpott, C. Rogers, O. Fedorov, M. Liu, W. Akhtar, A. Hayes, F. Raynaud, S. Müller, S. Knapp, S. Hoelder, *J. Med. Chem.* **2015**, *58*, 2553–2559.

[9] D. Spiliotopoulos, E. C. Wamhoff, G. Lolli, C. Rademacher, A. Caflisch, *Eur. J. Med. Chem.* **2017**, *139*, 564–572.

[10] J. R. Marchand, G. Lolli, A. Caflisch, *J. Med. Chem.* **2016**, *59*, 9919–9927.

[11] A. Unzue, H. Zhao, G. Lolli, J. Dong, J. Zhu, M. Zechner, A. Dolbois, A. Caflisch, C. Nevado, *J. Med. Chem.* **2016**, *59*, 3087–3097.

[12] N. Majeux, M. Scarsi, J. Apostolakis, C. Ehrhardt, A. Caflisch, *Proteins Struct. Funct. Bioinf.* **1999**, *37*, 88–105.

[13] N. Majeux, M. Scarsi, A. Caflisch, *Proteins Struct. Funct. Bioinf.* **2001**, *42*, 256–268.

[14] D. Spiliotopoulos, J. Zhu, E. C. Wamhoff, N. Deerain, J. R. Marchand, J. Aretz, C. Rademacher, A. Caflisch, *Bioorg. Med. Chem. Lett.* **2017**, *27*, 2472–2478.

[15] T. D. Crawford, V. Tsui, E. M. Flynn, S. Wang, A. M. Taylor, A. Cote, J. E. Audia, M. H. Beresini, D. J. Burdick, R. Cummings, L. A. Dakin, M. Duplessis, A. C. Good, M. C. Hewitt, H. R. Huang, H. Jayaram, J. R. Kiefer, Y. Jiang, J. Murray, C. G. Nasveschuk, E. Pardo, F. Poy, F. A. Romero, Y. Tang, J. Wang, Z. Xu, L. E. Zawadzke, X. Zhu, B. K. Albrecht, S. R. Magnuson, S. Bellon, A. G. Cochran, *J. Med. Chem.* **2016**, *59*, 5391–5402.

[16] M. Tanaka, J. M. Roberts, H. S. Seo, A. Souza, J. Paulk, T. G. Scott, S. L. De Angelo, S. Dhe-Paganon, J. E. Bradner, *Nat. Chem. Biol.* **2016**, *12*, 1089–1096.

[17] N. H. Theodoulou, P. Bamborough, A. J. Bannister, I. Becher, R. A. Bit, K. H. Che, C. W. Chung, A. Dittmann, G. Drewes, D. H. Drewry, L. Gordon, P. Grandi, M. Leveridge, M. Lindon, A. M. Michon, J. Molnar, S. C. Robson, N. C. O. Tomkinson, T. Kouzarides, R. K. Prinjha, P. G. Humphreys, *J. Med. Chem.* **2016**, *59*, 1425–1439.

[18] G. Lolli, A. Caflisch, *ACS Chem. Biol.* **2016**, *11*, 800–807.

[19] J. Zhu, A. Caflisch, *J. Med. Chem.* **2016**, *59*, 5555–5561.

[20] J. R. Marchand, A. Caflisch, *ChemMedChem* **2015**, *10*, 1327–1333.

[21] C. Tallant, E. Valentini, O. Fedorov, L. Overvoorde, F. M. Ferguson, P. Filippakopoulos, D. I. Svergun, S. Knapp, A. Ciulli, *Structure* **2015**, *23*, 80–92.

[22] G. Landrum, RDKit: Open-source cheminformatics, http://rdkit.org.

[23] K. Vanommeslaeghe, A. D. MacKerell, Jr., *J. Chem. Inf. Model.* **2012**, *52*, 3144–3154.

[24] K. Vanommeslaeghe, E. P. Raman, A. D. MacKerell, Jr., *J. Chem. Inf. Model.* **2012**, *52*, 3155–3168.

[25] M. Scarsi, J. Apostolakis, A. Caflisch, *J. Phys. Chem. A* **1997**, *101*, 8098–8106.

[26] M. Philpott, J. Yang, T. Tumber, O. Fedorov, S. Uttarkar, P. Filippakopoulos, S. Picaud, T. Keates, I. Felletar, A. Ciulli, S. Knapp, T. D. Heightman, *Mol. BioSyst.* **2011**, *7*, 2899–2908.

[27] V. G. D'Agostino, P. Lal, B. Mantelli, C. Tiedje, C. Zucal, N. Thongon, M. Gaestel, E. Latorre, L. Marinelli, P. Seneci, M. Amadio, A. Provenzani, *Sci. Rep.* **2015**, *5*, 16478.

[28] E. Quinn, L. Wodicka, P. Ciceri, G. Pallares, E. Pickle, A. Torrey, J. Hunt, D. Treiber, *Cancer Res.* **2013**, *73*, 4238.

[29] J. R. Marchand, A. Dalle Vedove, G. Lolli, A. Caflisch, *J. Chem. Inf. Model.* **2017**, *57*, 2584–2597.

[30] G. Lolli, R. Battistutta, *Acta Crystallogr. Sect. D* **2013**, *69*, 2161–2164.

[31] W. Kabsch, *Acta Crystallogr. Sect. D* **2010**, *66*, 125–132.

[32] P. R. Evans, G. N. Murshudov, *Acta Crystallogr. Sect. D* **2013**, *69*, 1204–1214.

[33] P. A. Karplus, K. Diederichs, *Curr. Opin. Struct. Biol.* **2015**, *34*, 60–68.

[34] A. J. McCoy, R. W. Grosse-Kunstleve, P. D. Adams, M. D. Winn, L. C. Storoni, R. J. Read, *J. Appl. Crystallogr.* **2007**, *40*, 658–674.

[35] P. D. Adams, P. V. Afonine, G. Bunkoczi, V. B. Chen, I. W. Davis, N. Echols, J. J. Headd, L. W. Hung, G. J. Kapral, R. W. Grosse-Kunstleve, A. J. McCoy, N. W. Moriarty, R. Oeffner, R. J. Read, D. C. Richardson, J. S. Richardson, T. C. Terwilliger, P. H. Zwart, *Acta Crystallogr. Sect. D* **2010**, *66*, 213–221.

[36] P. Emsley, B. Lohkamp, W. G. Scott, K. Cowtan, *Acta Crystallogr. Sect. D* **2010**, *66*, 486–501.